ACS APPLIED MATERIALS & INTERFACES

Research Article

www.acsami.org

Nanostructured Polystyrene Well Plates Allow Unbiased High-Throughput Characterization of Circulating Tumor Cells

Yuan Wan,[†] Marnie Winter,[†] Bahman Delalat,[‡] Jennifer E. Hardingham,[§,∥] Phulwinder K. Grover,[§] Joseph Wrin,[§] Nicolas H. Voelcker,[‡] Timothy J. Price,[§] and Benjamin Thierry*[,†]

[†]Ian Wark Research Institute, University of South Australia, Mawson Lakes, Adelaide, South Australia 5095, Australia

[‡]ARC Centre of Excellence in Convergent Bio-Nano Science and Technology, Mawson Institute, University of South Australia, Mawson Lakes, Adelaide, South Australia 5095, Australia

[§]The Queen Elizabeth Hospital and University of Adelaide, Adelaide, South Australia 5011 Australia

[∥]School of Medical Sciences, University of Adelaide, Adelaide, South Australia 5095, Australia

ABSTRACT: Rapid, reliable and unbiased circulating tumor cell (CTC) isolation and molecular characterization methods are urgently required for implementation in routine clinical diagnostic and prognostic procedures. We report on the development of a novel unbiased CTC detection approach that combines high-throughput automated microscopy with a simple yet efficient approach for achieving a high level of tumor cell binding in standard tissue culture polystyrene (PS) well plates. A single 5 min high-power oxygen plasma treatment was used to create homogeneous nanoscale roughness on standard PS tissue culture plates and, in turn, drastically enhance the binding of a range of tumor cells. After physical adsorption of an adlayer of poly-L-lysine, binding yields above 97% were obtained at 2 h for all tumor cell lines used in the study. Morphological analysis of the cells confirmed strong adherence to the nanorough PS substrates. Clinically relevant concentrations of a highly metastatic breast cancer cell line, used as model for CTCs, could be reliably detected among blood cells on the nanorough polystyrene plates using an automated microscopy system. The approach was then successfully used to detect CTCs in the blood of a stage IIIc colorectal cancer patient. By combining the high binding abilities of nanorough PS well plates with the high-throughput nature of high-content analysis systems, this methodology has great potential toward enabling unbiased routine clinical analysis of CTCs. It could be applied, once clinically validated, in any clinical center equipped with an automated microscopy facility at a fraction of the cost of current CTC isolation technologies.

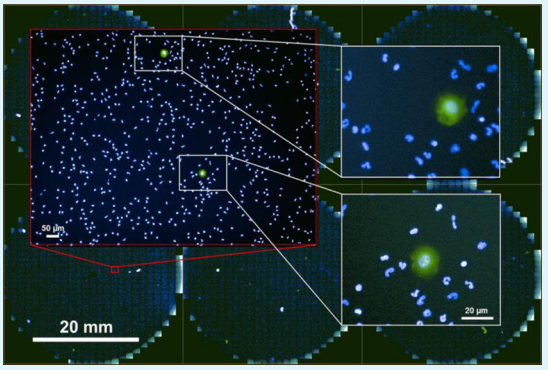

KEYWORDS: *circulating tumor cells, polystyrene, nanostructure, oxygen plasma, high throughput microscopy, colorectal cancer*

1. INTRODUCTION

The isolation and analysis of circulating tumor cells (CTCs) from cancer patient blood, often referred to as a "liquid biopsy", can provide important diagnostic and prognostic information.[1−3] For example, enumeration of CTCs is a prognosticator in patients with early stage and metastatic breast cancer.[4] Dynamic changes in CTC loads can also serve as a surrogate biomarker for the assessment of therapeutic efficacy.[5] In addition, molecular analysis of CTCs provides a window into the pathophysiology of metastatic diseases and thus offers the possibility of monitoring changes in tumor genotypes and guiding anticancer treatment regimens.[2,6−8]

A number of approaches have been reported for the detection and isolation of CTCs.[9−11] In general, these methods fall into two categories: biological methods based on affinity-isolation of the target cells and physicochemical methods. Approaches based on affinity interactions provide very high specificity and efficiency in isolating cells expressing targeted biomarkers.[12] However, because there is currently no ubiquitous biomarker that can be used to isolate CTCs, biological methods are inherently biased. Of major concern, for instance, is the occurrence of epithelial to mesenchymal transition (EMT) in CTCs. CTCs with EMT-like phenotype may indeed not express the epithelial cell adhesion marker (EpCAM), the transmembrane glycoprotein most widely used in affinity-based CTCs isolation approaches.[13] Low or complete lack of EpCAM expression can be expected to result in false-negative findings.[14,15] In addition, in certain scenarios CTCs need to be detached from the isolation platform for further in vitro cell culture. Efficient detachment of viable immuno-captured CTCs poses a major postisolation challenge.[16]

In contrast, physicochemical methods exploit differences in size, deformability, and electrical properties between CTCs and nucleated blood cells. Although isolation purity from physical

Received: August 4, 2014
Accepted: November 4, 2014
Published: November 4, 2014

methods is typically lower than that of biological methods (<10%), they are highly efficient (>90%), label-free, and provide great flexibility in subsequent enumeration and molecular profiling of CTCs.[10] It is generally assumed that CTCs are larger than nucleated blood cells, and this assumption forms the basis of size-based isolation methods; however, CTCs at different stages of apoptosis or in a dormant state are expected to have smaller size.[17] Potential morphological changes associated with EMT also remain to be investigated. In addition, the issue of CTC deformability is controversial, as opposite observations have been reported.[18,19] Thus, the performance in clinical settings of current physical isolation methods, such as isolation by size of epithelial tumor cells (ISET),[20] micropore chip,[21] and CellSievo,[22] is likely to be lower than predicted from model studies with tumor cell lines. Furthermore, despite tremendous advances in this field, both biological and physical isolation methods usually remain expensive and time- and resource-consuming, which limits their applicability to clinical uses. Rapid, affordable, and reliable unbiased CTC isolation methods for subsequent enumeration and characterization are still urgently required toward the establishment of clinically relevant CTC-based prognostic and diagnostic strategies.

As an alternative to enrichment technologies, high-throughput automated microscopic analysis of the whole nucleated cellular population in a blood sample is attractive because it has the potential to provide the required unbiased sensitive detection of CTCs. Recent developments in high-content imaging platforms enable rapid molecular and morphological characterization of a large number of cells and commercial platforms have been already developed for CTCs enumeration.[23] To fulfill their clinical potential, such high-content screening approaches will require the development of substrates able to efficiently bind tumor cells present in a blood sample while also being compatible with automated microscopy. Nanostructured substrates that mimic the structural features of the extracellular matrix or basement membrane have recently been successfully employed in CTCs isolation and detection.[24] Combined with biological ligands, nanostructured substrates provide a high surface area for ligand immobilization while lowering the rolling velocity of cells in microfluidic channels and, in turn, increasing isolation yields. It has been recently reported that tumor cells have very high binding affinity on nanostructured surface, even without functionalization with biological ligands, owing to the dynamic arrangement of integrin-mediated focal adhesions.[25] Nanostructured substrates are therefore a promising label-free bioplatform for CTC isolation. Due to the limitation of existing nanofabrication methods, large-scale fabrication of homogeneous nanostructured substrates is, however, nontrivial and also associated with high fabrication costs. Thus, the main limitation of reported nanostructure-based CTC isolation techniques is that they can typically only process a limited amount of blood at a time (<0.5 mL). Screening CTCs from high volumes of blood (up to 60 mL) would be optimal to provide a true liquid biopsy for solid cancers.[26] However, in the clinical setting relevant CTC isolation approaches should be able to process rapidly and efficiently about ∼5−10 mL of blood, especially when considering the small number of CTCs present, especially in early stage cancer patients.

We report here on an integrated CTC detection approach combining high-throughput total content screening technology with a simple yet efficient method to significantly increase tumor cell binding on standard tissue culture polystyrene well plates. More specifically, we demonstrate that a single 5 min high-power oxygen plasma treatment creates homogeneous nanoscale roughness on standard tissue culture polystyrene substrates and, in turn, drastically enhances the binding of a range of tumor cells. Oxygen plasma treatment of polystyrene (PS) has been widely used since the 1990s to create optimal surface for tissue culture.[27] Adherent cells can indeed efficiently bind and proliferate on the resulting hydrophilic PS surface.[28] This proposed approach enabled rapid, unbiased detection and molecular analysis of tumor cells spiked in low concentrations in peripheral blood. Considering the growing availability of automated microscopy facilities, nanostructured polystyrene well plates as described here have a strong potential to provide a much-needed technological solution toward large-scale clinical implementation of CTC-based diagnostic and prognostic strategies.

2. MATERIALS AND METHODS

All chemicals were obtained from Sigma-Aldrich, unless otherwise noted.

2.1. Oxygen Plasma Treatment and Surface Characterization. Six-well plates (standard Corning Costar 3516) were exposed to oxygen plasma (Plasma asher, Siemens) at 500 W for 5, 10, and 15 min at a pressure of 0.1 mbars with a 100 mL/s oxygen flow rate. To introduce a dense layer of NH_2 functionalities on the surface, freshly plasma-treated PS wells were incubated with a 0.01% (w/v) poly-L-lysine (PLL) solution (MW: 150, 000−300, 000) in deionized (DI) water for 2 h at RT. After a thorough rinsing with DI water and 1× PBS, the plates were dried with a nitrogen stream.

Surface topography was evaluated quantitatively using a JPK atomic force microscope (AFM). Changes in surface area and root-mean-square surface roughness (R_q) were measured. Height image of samples were captured in ambient air with 15−20% humidity in the tapping model. The analyzed field was 1 × 1 μm, and images were acquired at a scan rate of 1 Hz with 256 scanning lines. Water contact angles were measured on PS before and after plasma treatment. A droplet of DI water was placed on the surface of the substrate at room temperature (RT), and after 30 s, the contact angle was measured using a contact angle goniometer (NRL-100, Rame-Hart). Typically, five measurements were averaged for each run. The surface chemistry of the samples was characterized using X-ray photoelectron spectroscopy (XPS) using a Kratos AXIS Ultra DLD X-ray photoelectron spectrometer with a monochromatic Al Kα X-ray source and a hemispherical analyzer. The pass energy was 20 eV with a resolution of 0.3 eV for high-resolution spectra. Spectra were collected at a photoelectron takeoff angle of 90°. Binding energies were referenced to the C 1s hydrocarbon carbon peak at 285.0 eV to compensate for surface charging effects.

2.2. Cell Culture. BSR, HEK293, 3T3, SH-SY5Y, T98G, MCF7, MDA-MB231, MDA-MB231 HM, and EMT6 cell lines were cultured in Dulbecco's modified Eagle's medium (DMEM) supplemented with 10% FBS; penicillin, 100 U/mL; streptomycin, 100 μg/mL; and plated in T-25 tissue culture flasks. Flasks were placed into an incubator maintained 5% CO_2 at 37 °C and 10% humidity. A highly metastatic variant of the MDA-MB231 breast cancer cell lines (MDA-MB-231-HM) initially reported by Prof. Zhou-Luo Ou (Fudan University Shanghai Cancer Center, China) was provided by Dr. Erica Sloan (Monash University). The MDA-MB-231-HM cells were transfected with a lentiviral vector for green fluorescent protein (GFP).

2.3. Tumor Cell Binding Yields. To determine the yield of binding on the various PS samples, we used a range of tumor cell concentrations (from 1×10^2 to 5×10^5 cells/mL). Cells suspended in DMEM were added into the treated PS wells, which had been first sterilized using 70% ethanol and incubated for 0.5, 1, 2, 4, and 6 h. The wells were washed gently to remove unbound cells and the attached cells were fixed with 4% paraformaldehyde for 1 h at RT. Twenty representative images (×10) were randomly taken for each sample

with a Nikon TE inverted microscope. Cell numbers per images were manually counted and the resulting cell densities calculated and expressed as number of cells per mm^2. The binding yield was defined as the number of cells bound to the PS wells divided by the initial seeded cell number. The cell morphology was also recorded, and the percentage of cells with a flat morphology was calculated as described previously.[29,30]

2.4. Tumor Cell Isolation Yields from Blood. To accurately determine the isolation yield, we spiked MDA-MB231 HM cells stably transfected to express GFP into healthy blood. The GFP expression rate of the MDA-MB231 HM cells was first calculated and was approximately 99%. This value was used to correct isolation yields. Then, 200, 400, and 800 μL of 2.5×10^2 cells/mL MDA-MB231 HM cells were spiked in 1 mL of fresh healthy human blood ($n = 3$); 1 mL of the spiked sample was mixed with 14 mL cold red blood cell (RBC) lysis buffer (containing 15.5 mM NH_4Cl, 0.1 mM EDTA, and 1 mM $NaHCO_3$) for 10 min at RT. Nucleated cells, including WBCs, and the spiked cancer cells were washed by centrifugation at 4 °C for 5 min at 250*g* and resuspended in DMEM culture medium. The cellular mixtures were added to the treated PS well plates and incubated for 2 h. The typical total cell density on the PS surface was about 1000 cells/mm^2. MDA-MB231 HM cells expressing GFP could be readily detected using fluorescent microscopy. Well plates were analyzed using the Operetta (PerkinElmer, Waltham, MA) high-content imaging system using 10× and 20× objectives. MDA-MB231 HM cells isolated in every well were counted, and a linear regression analysis between the detected numbers and the spiked numbers was performed.

Next, to demonstrate the feasibility of immunostaining the isolated cells, were also used nonfluorescent MCF7. After we isolated the cells as described above, we stained the cells with an Anti-Human CD45 FITC. After a washing step with basic buffer (1× PBS and 0.5% sodium azide), cells were fixed with 4% paraformaldehyde for 1 h at RT and then sequentially treated with permeabilizing block buffer (1× PBS with 0.5% sodium azide supplemented with 0.05% Triton X-100 and 10% FBS) and 10 μg/mL of anticytokeratin (AE1/AE3) eFluor 660 for 30 min on ice. Cells were then washed with perm wash (basic buffer supplemented with 0.05% Triton X-100) three times followed by 0.1 μg/mL DAPI staining.

2.5. Tumor Cell Retention during Staining. To determine the loss of tumor cells during immuno-staining, we seeded 2 mL of 2.5×10^4 cells/mL pretreated with the cell lysing buffer, as described before for MCF7 cells, into either a PLL-treated nanorough PS well plate or into an untreated one. Cells were allowed to bind for 2 h and then subjected to the staining procedure. Cell loss was determined by counting cell numbers in 8×1 mm^2 areas randomly selected before and after applying the complete staining procedure.

2.6. Detection of CTCs in Blood of Colorectal Cancer Patient. Human ethics approval was obtained from the ethics committee of The Queen Elizabeth Hospital. Following approval, 7.5 mL of peripheral blood was collected from a stage IIIc colorectal cancer patient. The blood sample was lysed as described above, and the cells were plated on the roughened plates and then stained with anti-Human CD45, anti-CK, antivimentin eFluor 570, and DAPI. Typically, 6-well plates were analyzed using the Operetta system using 10× and 20× objectives.

3. RESULTS AND DISCUSSION

3.1. Oxygen Plasma Treatment of PS. PS samples treated for 15 min were typically deformed as a result of the elevated temperature induced by the high-powered atomic oxygen attack during the plasma treatment. The glass transition temperature of PS is approximately 100 °C,[31] which limits the temperatures to which PS samples can be exposed. It was noted that even for 10 min of treatment, the PS plates occasionally distorted. The morphology and surface roughness of the oxygen-plasma-treated PS was characterized using AFM. As shown in Figure 1, homogeneously distributed nanostructured

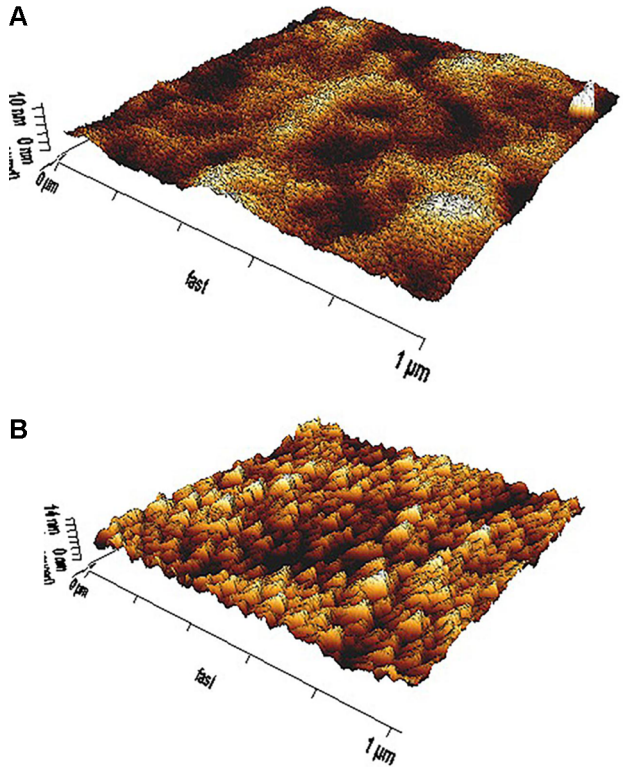

Figure 1. Representative AFM images (1×1 μm) of (A) untreated PS and (B) PS treated with 500 W oxygen plasma for 5 min. The surface roughness increased from 0.85 nm for untreated PS to 4.26 nm for the nanostructured plasma treated PS surface.

features were generated on the standard tissue culture PS substrates used in this study following high-powered oxygen plasma treatment. Surface features with low aspect ratios and pyramidal shapes with approximately 60 nm lengths of bottom line and 14 nm heights were obtained. The surface roughness increased with increasing exposure times. The R_q values of untreated PS, 5 min treated PS, and 10 min treated PS were 0.85 nm (SD: 0.14 nm), 4.26 nm (SD: 0.23 nm), and 4.49 nm (SD: 0.09 nm), respectively. Considering the only modest increase in roughness resulted from prolonged treatment with high powered oxygen plasma, 5 min plasma treatment was therefore selected and applied for the rest of the study. XPS elemental analysis showed a significant increase in the oxygen percentage on the PS samples from 14.2 to 25%, confirming that the expected oxidation of the PS surface took place during the oxygen plasma (Figure 2A). Next, the water contact angles of PS samples treated for 5 min with the high-powered oxygen plasma were continuously monitored for 72 h, and the average values and standard deviations were recorded. Static water contact angle decreased from $52 \pm 3°$ for untreated PS to be undetectably low for oxygen-plasma-treated PS (typically measured within 20 min of the plasma treatment). Contact angles increased to $3 \pm 1°$ at the 24 h time point, $9 \pm 1°$ at the 48 h time point, and $11 \pm 2°$ at the 72 h time point. These measurements show that the high-power oxygen plasma treatment enables PS to remain superhydrophilic for at least 72 h.

3.2. Tumor Cell Binding Yields. Our data demonstrates that a 5 min oxygen plasma treatment at high power significantly increases the roughness of standard tissue culture PS, thereby resulting in homogeneously nanostructured

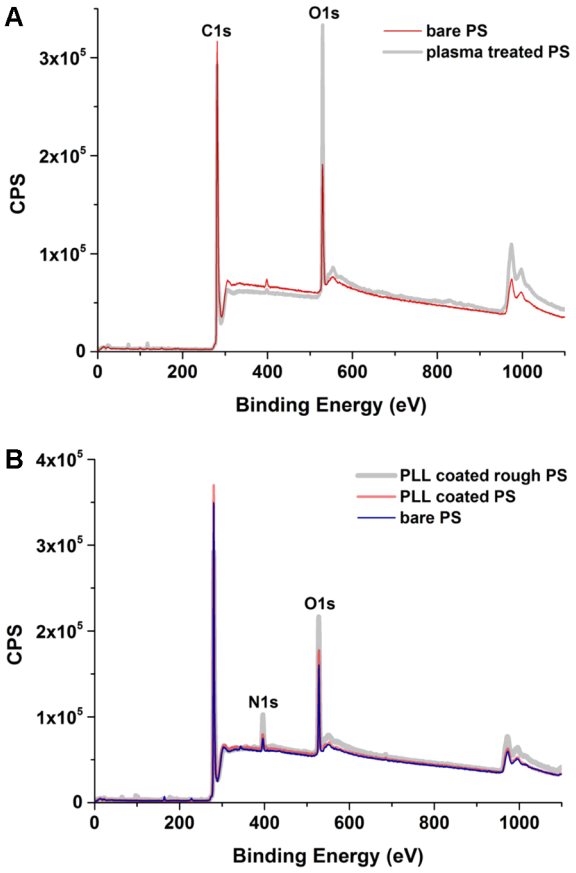

Figure 2. (A) XPS elemental analysis of (gray line) untreated and (red line) oxygen-plasma-treated PS samples. (B) XPS elemental analysis of untreated PS, PLL adsorbed on untreated PS, and PLL adsorbed on oxygen-plasma-treated PS.

surfaces. To determine the effect of the nanoscale roughness, 5 × 10^5 T98G (glioblastoma cell line) cells suspended in DMEM were incubated on various substrates including plasma treated PS (rough PS), untreated PS (PS), as well as glass used as control for low adhesion for up to 6 h. T98G cell binding yields increased in all three groups with extended incubation time (Figure 3A). At the 2 h time point, for instance, 94 ± 2% of the cells had adhered onto the rough PS while only 73 ± 2.5% and 34 ± 4% cells were bound onto the untreated PS and glass surface, respectively. These results demonstrate that as expected the use of nanostructured PS could significantly accelerate the binding of the T98G tumor cells. The latter likely originate in the increased roughness and hydrophilicity of the treated PS, offering larger surface area for cell attachment and spreading.[28] To further characterize the binding yields, we investigated cell seeding numbers ranging from 10^2 to 5 × 10^5 T98G cells per mL. An average of 94% binding efficiency at the 2 h time point was observed for the rough PS group, showing a reliable constant sensitivity (Figure 3B). Higher variations were observed for the lower seeding concentrations, which was mainly due to the inherent error associated with manipulation of low cell numbers.

Although the binding yield of the T98G cells on rough PS was increased to 98 ± 3% at the 6 h time point, short incubation times are preferable toward practical implementation in routine clinical work. In addition, it has been reported that a significant percentage of CTCs are in different stages of apoptosis;[32] and CTCs presenting both mild apoptotic changes, such as cytoplasmic blebbing, and apoptotic indicators in the nucleus have been observed.[23] CTCs can be expected to initiate an apoptosis program during longer incubation time in vitro and consequently have reduced binding during the assay. Therefore, rapid attachment of cells onto the substrate is preferred. On the basis of these considerations and the binding yield results, we selected a 2 h incubation time as a good compromise.

Oxygen plasma treatment is a well-established methodology to modify the surface morphology of polymeric materials and increase their roughness. For instance, oxygen plasma was used to introduce nanoscale roughness on polyethylene terephthalate and, in turn, drastically influenced the adhesion of mouse liver cancer cells.[33] Tumor cells significantly proliferated on nanostructured surfaces with a low aspect ratio due to enhanced mechanical anchoring; in contrast, superhydrophilic surfaces with high aspect ratio nanostructures failed to offer sufficient sites for focal adhesion and thus suppressed the adhesion and growth of the mouse liver cancer cells. A template approach was recently used to prepare nanostructured PS, which was found to efficiently bind tumor cells.[34] Although advanced fabrication technology such as reactive ion etching can be used to prepare nanorough surfaces with exquisite control over the morphology of the nanoscale features, oxygen plasma is rapid, cost-efficient, and readily available in most research environments. While further studies are required to fully understand the structure−activity relationships of nanostructured surfaces in regard to cell adhesion, high-power oxygen plasma treatment of PS is a simple yet efficient approach to introduce homogeneous nanoscale roughness and foster tumor cell binding.

Next, the binding yields on the nanorough PS of eight different types of cells, including three of noncancerous cell lines (BSR, HEK293 and 3T3), were determined. In agreement with the data obtained for T98G cells, high binding yields were observed for tumor cells (over 91% for all tested cells) on the rough PS after 2 h incubation; in contrast, only 76% of HEK293 cells were bound onto nanorough PS, which is consistent to the inherently weak adhesion ability of this cell line (Figure 3C). However, for even the HEK293 cells, the binding yield was significantly enhanced on the rough PS surface because less than 40% adhered to the untreated tissue culture PS at the 2 h time point. The cellular morphology can reflect the level of cell adhesion. In general, higher contact area between cells and substrates, along with flatter morphology (changed from a globular shape to a semielliptical one) with decreased height is typically linked to strong attachment to the substrate.[35] On the contrary, a refractile and rounded cellular morphology indicates relatively weak attachment, which may lead to detachment under high shear stress, for instance during the washing steps associated with immunostaining of the cells. To further investigate this aspect, cells adhered to the PS substrate were observed in bright field microscopy, and cells with obvious lamellipodia or filopodia were defined as cells with "flat morphology". At least 80% of the attached cells were classified as flat except for the HEK293 cells (Figure 3D); over 90% of the SH-SY5Y (neuroblastoma cell line) and T98G cells displayed flat morphologies.

These results demonstrate that the tumor cell lines used here all had efficient, strong, and rapid attachment onto tissue culture PS treated with 5 min of high-powered oxygen plasma. However, approximately 3−7% of the tested cancer cells did not attach onto the rough PS at the 2 h time point target. In

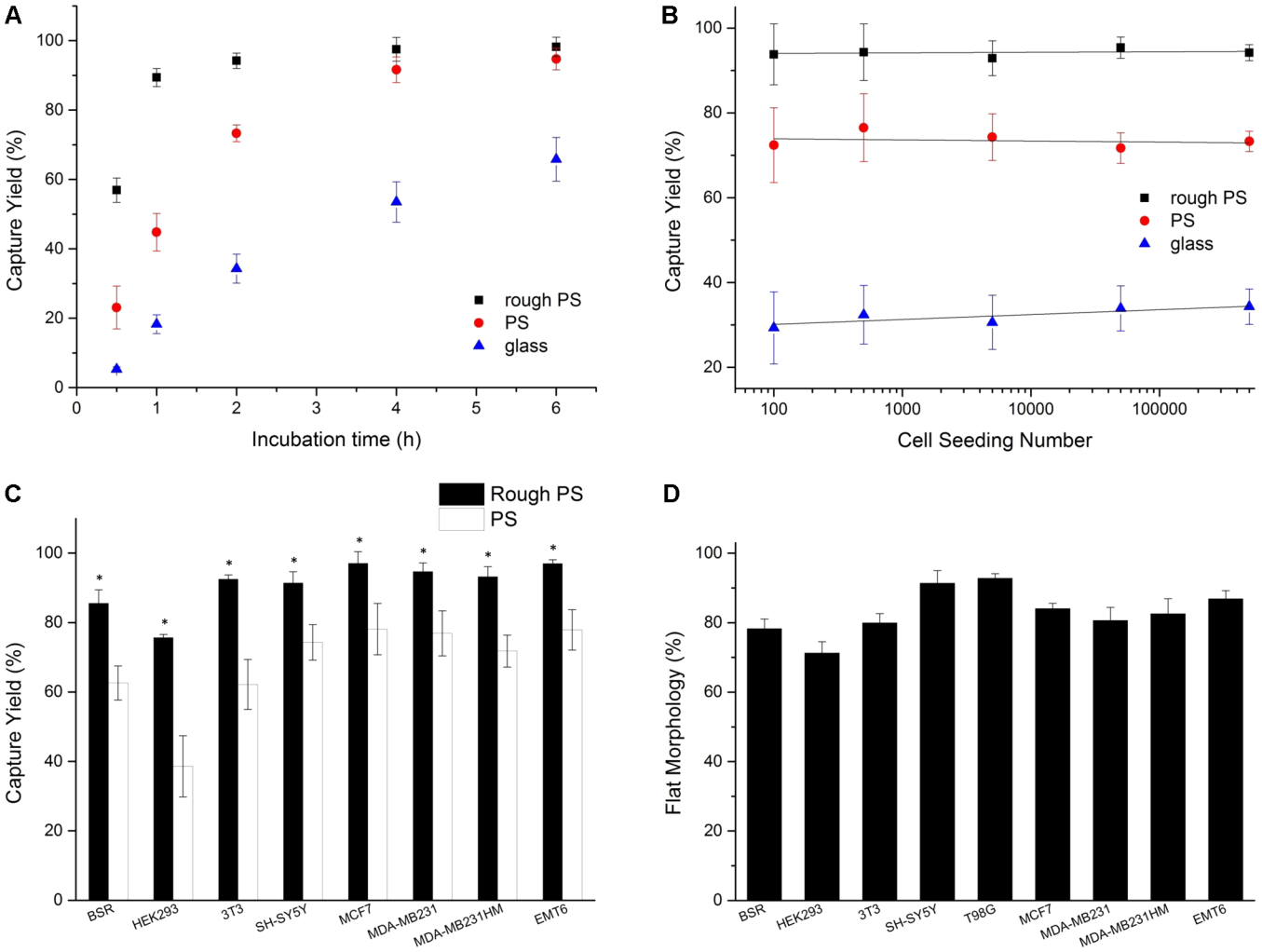

Figure 3. (A) Binding yields of T98G cells as a function of incubation time on untreated PS, oxygen plasma rough PS, and glass. (B) Binding yields at 2 h as a function of seeding density for T98G cells on untreated PS, oxygen plasma rough PS, and glass. (C) Binding yields for different cell lines on untreated PS and oxygen plasma rough PS. For each group, 5×10^5 cells were seeded and incubated at 37 °C for 2 h (*, $p < 0.05$). (D) Percentage of cells with flat morphology on rough PS substrates. For each group, 5×10^5 cells were seeded and incubated at 37 °C for 2 h.

addition, the exact phenotype of CTCs is not yet fully determined, and consequently, cancer cell lines cannot fully represent CTCs. Phenotypical changes have indeed been observed along with a high level of heterogeneity. The presence of a significant percentage of apoptotic CTCs is also an issue, although the clinical relevance of these cells remains to be established. Toward further improving the binding yield of tumor cells on the rough PS, the addition of an electrostatic layer based on poly-L-lysine (PLL) resulting in excess positive charges on the surface was investigated. PLL is commonly used in cell biology to create positively charged surfaces, which enhance binding to negatively charged cellular membranes. Freshly oxygen-plasma-treated PS samples were incubated with a PLL aqueous solution and thoroughly washed with PBS. XPS analysis was used to confirm the presence of the PLL layer onto the PS. As shown in Figure 2, XPS elemental spectra revealed a significant increase in the peak at 400 eV attributed to N 1s (6.5%) for PS samples treated for 5 min with oxygen plasma and incubated with PLL in comparison to untreated PS (2.7%). No significant increase in elemental nitrogen percentage was detected after incubating untreated PS with PLL (N 1s = 2.6%). The significant increase in elemental nitrogen on the surface confirmed the adsorption of the polyamino acid on the surface of the plasma oxygen treated PS. Next, the binding yields and cellular morphology on PLL-treated nanorough PS was determined. For all six types of cancer cells on PLL-coated rough PS, binding yields were increased in comparison to the non-PLL-coated samples and reached almost 100% at the 2 h time point (Figure 4). In addition, all the cells adhered to the surface displayed visible lamellipodia or filopodia.

Finally, the binding yield on the PLL-coated rough PS substrates of pure WBCs collected from 1 mL peripheral healthy blood was also investigated. Binding yields close to 100% were observed, similar to that of cancer cells, at the 2 h time point. This result confirmed that the combination of excess positive charges resulting from the PLL adsorbed layer and the nanorough features introduced on the PS by high-powered oxygen plasma is highly efficient to ensure strong and rapid binding of both a wide range of tumor cell lines and WBCs isolated from blood.

3.3. Isolation and Detection of Tumor Cells from Blood Using Treated PS and Automated Microscopy. Having established a simple and robust protocol to significantly increase the binding of tumor cells on standard tissue culture PS well plates, its compatibility with high-throughput detection of tumor cells from peripheral blood using automated

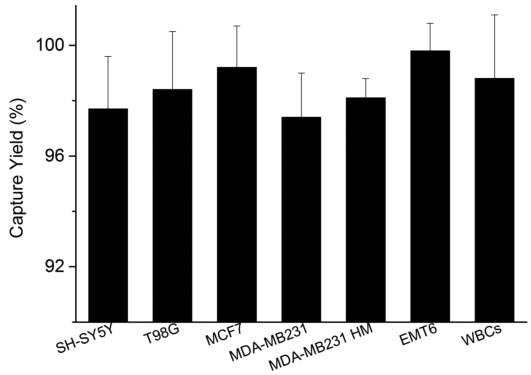

Figure 4. Binding yields for different cell lines on PLL rough PS. For each group, 5×10^5 cells were seeded and incubated at 37 °C for 2 h.

microscopy was determined. To this end, a high content analysis system was used (Operetta, PerkinElmer) to automatically screen the PS well plates. Six well plates were first treated for 5 min with high-powered oxygen plasma and further reacted with PLL, as described. A highly metastatic variant of the human breast cancer cell lines MDA-MBA231 transfected to stably express the green fluorescent protein was used to model CTCs (MDA-MB231-HM).[36] The MDA-MB231 HM cells were carefully spiked into blood collected from a healthy donor at known concentrations (50, 100, and 200 cells per mL).

The blood samples were subjected to standard lysis, resuspended in DMEM medium, and finally seeded into the PLL coated rough PS well plates. After 2 h of incubation, the well plates were washed with PBS and imaged using the Operetta system. The number of fluorescent MDA-MB231-HM cells detected in the wells is shown in Table 1, and

Table 1. Enumeration of MDA-MB231 HM Cells Spiked in Whole Blood on PLL-Coated Rough PS Using the Operetta System

sample	number of spiked cells (based on calculation)	number of detected cells (based on fluorescence detection)	calibrated value	detection rate (%)
1a	50	45	45.5	91
1b	50	56	56.6	113.2
1c	50	46	46.5	93
2a	100	109	110.2	110.2
2b	100	91	92	91
2c	100	114	115.3	115.3
3a	200	207	209.3	104.7
3b	200	213	215.4	107.7
3c	200	202	204.3	102.2

representative images of the cells are shown in Figure 5. The number of detected cells was within the experimental error inherent to ultralow cell numbers and consistent with the number of spiked cells, and a good correlation was calculated using a simple regression analysis (R^2 = 0.99) demonstrating quasi complete binding of the MDA-MB231-HM cells spiked in the blood in this assay. With a 20× magnification, the morphology of the attached cancer cells was easily observed, and the presence of lamellipodia evidenced strong binding to the treated PS substrates. High content screening technologies have rapidly progressed in recent years, providing powerful means to screen a large number of cells and obtain multiparametric characterization. Several commercial platforms

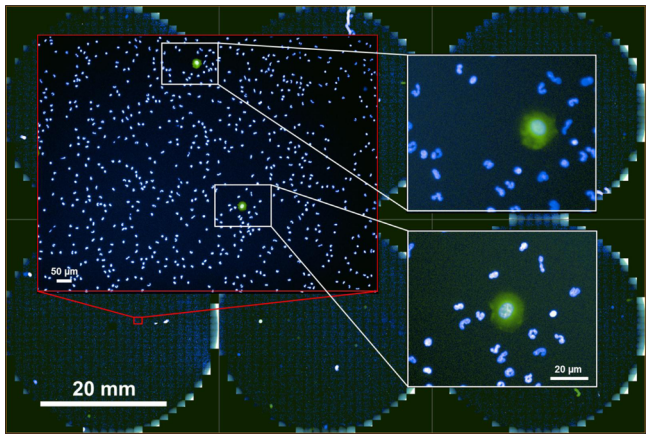

Figure 5. MDA-MB231 HM cells were observed among WBCs in a 6-well plate. The panoramagram is composed of approximately 4000 images taken at 10× magnification. (Insets) The red box indicates a field of view obtained using the 10× objective lens and containing 2 MDA-MB231 HM cells; the white boxes indicate areas of magnification obtained using the 20× objective lens and clearly display the morphology of the cells on the PS substrate.

have been developed, and our results demonstrate the feasibility of high-throughput automated isolation and detection of tumor cells from peripheral blood using commercially available well plates. High-content screening systems such as the Operetta have the potential to provide advanced phenotypical and morphological characterization, which is a key requirement toward clinical implementation of CTCs in cancer diagnostic and prognostic applications.

Next, to confirm the feasibility of reliably quantification of tumor cells isolated from peripheral blood and demonstrate the possibility to carry out phenotypical characterization, we spiked nonfluorescent MCF7 cells in blood and isolated using the PLL rough PS approach. Cells were stained in the well plates using anti CD45 and anticytokeratin (AE1/AE3) antibodies and detected with the Operetta system, as shown in Figure 6. As

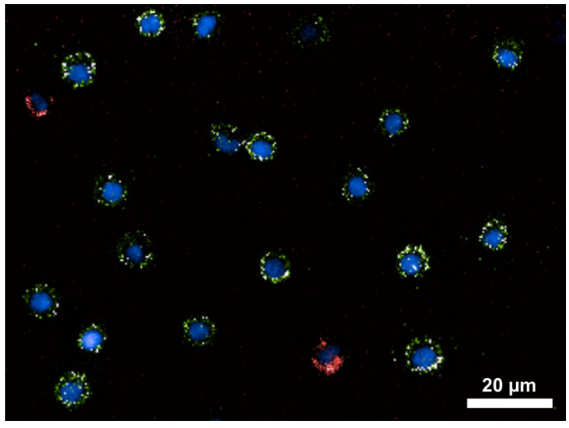

Figure 6. Positive DAPI and anti-CK staining of MCF7 cells isolated on the rough PS. The picture was taken using the 20× objective lens.

expected, MCF7 cells showed a strong specific cytoplasmic cytokeratin staining pattern, which was not observed on WBCs, thereby enabling their accurate quantification and characterization.

Next, the loss of tumor cells during staining was determined. MCF-7 cells treated with the lysing buffer were seeded on

either PLL-treated nanorough PS or in a control tissue culture PS well-plate and allowed to attach for 2 h. The cells were then washed and stained as described above. Cell retention on the PLL-treated nanorough PS was found to be 96 ± 3%. On the other hand, decreased cell retention was determined for cell seeded on untreated tissue culture PS (58 ± 17.5%). These results confirm the strong adhesion of tumor cells onto nanorough plasma-treated PS and demonstrate that only minimal cell loss occurs during staining, which is an important feature when considering very rare events.

3.4. Detection of CTCs from Colorectal Cancer Patient's Blood Sample. Finally, we aimed to validate a complete protocol for the detection of CTCs from patients' blood using the proposed rough PS well plates/automated microscopy approach. To this end, an important consideration is the binding capacity of the samples. From our experimental observation cell density within the PS wells should not be higher than 3000 cells/mm^2 to avoid steric issues and the resulting decrease of cell binding efficiency. With such considerations in mind, 3−4 mL of blood per plate could be reliably analyzed. To validate our approach, we collected blood from a colorectal cancer (stage IIIc) patient. Nucleated cells were obtained, seeded as described above, and stained and imaged with the Operetta system. To identify CTCs, we used the fluorescent markers anti-CD45, anticytokeratin, and antivimentin and coupled them with the cytomorphology as revealed using the 20× objective. Morphological examination can be useful in distinguishing background staining from the true CTCs,[37] and an inherent advantage of the proposed approach is the possibility of obtaining high-resolution images of the putative CTCs. Cells that showed a positive nuclear staining with DAPI, a negative staining against CD45, and a positive staining for CK were considered as CTCs (Figure 7).

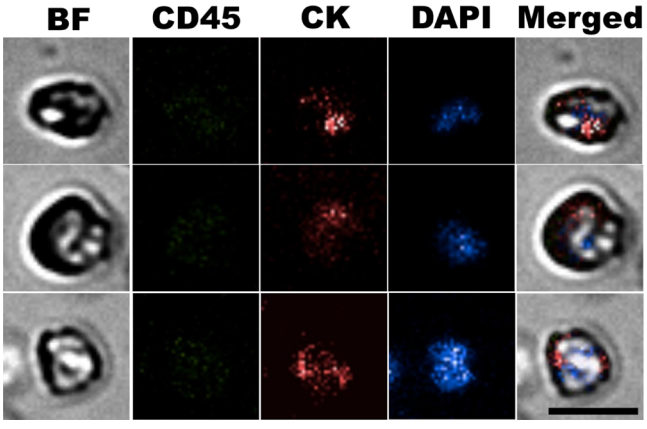

Figure 7. DAPI, CD45, and anticytokeratin staining of CTCs isolated from a colorectal cancer patient. A total of 21 CTCs were detected in 3.5 mL of peripheral blood. The picture was taken using the 20× objective lens. BF = bright field. The scale bar equals 10 μm.

To rule out false positive WBCs, we strictly excluded cells showing clear CD45-positive staining, even if these cells exhibited abnormal morphology and CK-positive staining. Twenty-one CTCs in the 3.5 mL of blood analyzed were unambiguously identified. No vimentin positive cells were observed. No cells with epithelial phenotype (CK) were detected in control experiments using blood from healthy donors.

Depending on the number of markers used to characterize the CTCs and the specifications of the microscopy platform, automated analysis could be completed as quickly as 2 h, giving a total isolation and analysis time of approximately 5 h from blood collection with minimum manipulations. The proposed approach is also expected to be compatible with current positive and negative CTC enrichment technologies, which could further shorten analysis times. For instance, leukapheresis was recently demonstrated as a clinically safe method to enrich and concentrate CTCs from large blood volume[26] and could be easily integrated into the proposed isolation/detection platform in the future. Finally, a number of commercial automated microscopy platforms are currently available at a fraction of the cost of current commercial CTCs detection systems.

4. CONCLUSION

In this study, we have demonstrated that a simple 5 min high-power oxygen plasma treatment introduces homogeneously distributed nanoscale features on standard tissue culture PS plates. The presence of the nanoscale roughness significantly increased the binding of a range of tumor cells, and morphological analysis demonstrated strong adherence of the cells to the nanorough PS substrates. Physical adsorption of an adlayer of poly-L-lysine resulted in a further modest increase in the binding yields. At least 97% binding yields were obtained at 2 h for all tumor cell lines investigated in the study. Using the Operetta automated high-content analysis system, clinically relevant concentrations of a highly metastatic breast cancer cell line spiked in peripheral blood could be reliably detected on the rough polystyrene plates. The proposed approach was successfully used to detect CTCs in the blood of a stage IIIc colorectal cancer patient, demonstrating its feasibility in a real-life situation. The highly efficient tumor cell isolation substrates reported here could be readily used, once clinically validated, on a large scale in any center equipped with automated microscopy facilities. This approach has the potential to provide a cost-effective technological solution toward large-scale clinical implementation of CTC-based diagnostic and prognostic strategies

AUTHOR INFORMATION

Corresponding Author

*E-mail: benjamin.thierry@unisa.edu.au.

Notes

The authors declare no competing financial interest.

ACKNOWLEDGMENTS

This work was supported by the National Health and Medical Research Council (NH&MRC) Project grant APP 631939. The authors would like to thank the Australian National Fabrication Facility (ANFF) node of South Australia for access to their facilities, as well as Prof. Zhou Luo Ou (Fudan University) and Dr. Erica Sloan (Monash University) for providing MDA-MB231-HM cells. Thanks also to Dr. Marco Herald at Walter and Eliza Hall Institute for the GFP lentiviral construct used to transfect the MDA-MB231-HM cells.

REFERENCES

(1) Alix-Panabieres, C.; Pantel, K. Circulating Tumor Cells: Liquid Biopsy of Cancer. *Clin. Chem.* **2013**, *59*, 110−118.

(2) Kang, Y.; Pantel, K. Tumor Cell Dissemination: Emerging Biological Insights from Animal Models and Cancer Patients. *Cancer Cell* **2013**, *23*, 573−581.

(3) van de Stolpe, A.; Pantel, K.; Sleijfer, S.; Terstappen, L. W.; den Toonder, J. M. Circulating Tumor Cell Isolation and Diagnostics: Toward Routine Clinical Use. *Cancer Res.* **2011**, *71*, 5955−5960.
(4) Zhang, L.; Riethdorf, S.; Wu, G.; Wang, T.; Yang, K.; Peng, G.; Liu, J.; Pantel, K. Meta-Analysis of the Prognostic Value of Circulating Tumor Cells in Breast Cancer. *Clin. Cancer Res.* **2012**, *18*, 5701−5710.
(5) Gorges, T. M.; Pantel, K. Circulating Tumor Cells as Therapy-Related Biomarkers in Cancer Patients. *Cancer Immunol. Immunother.* **2013**, *62*, 931−939.
(6) Joosse, S. A.; Pantel, K. Biologic Challenges in the Detection of Circulating Tumor Cells. *Cancer Res.* **2013**, *73*, 8−11.
(7) Yu, M.; Ting, D. T.; Stott, S. L.; Wittner, B. S.; Ozsolak, F.; Paul, S.; Ciciliano, J. C.; Smas, M. E.; Winokur, D.; Gilman, A. J.; Ulman, M. J.; Xega, K.; Contino, G.; Alagesan, B.; Brannigan, B. W.; Milos, P. M.; Ryan, D. P.; Sequist, L. V.; Bardeesy, N.; Ramaswamy, S.; Toner, M.; Maheswaran, S.; Haber, D. A. RNA Sequencing of Pancreatic Circulating Tumour Cells Implicates WNT Signalling in Metastasis. *Nature* **2012**, *487*, 510−513.
(8) Yu, M.; Bardia, A.; Wittner, B. S.; Stott, S. L.; Smas, M. E.; Ting, D. T.; Isakoff, S. J.; Ciciliano, J. C.; Wells, M. N.; Shah, A. M.; Concannon, K. F.; Donaldson, M. C.; Sequist, L. V.; Brachtel, E.; Sgroi, D.; Baselga, J.; Ramaswamy, S.; Toner, M.; Haber, D. A.; Maheswaran, S. Circulating Breast Tumor Cells Exhibit Dynamic Changes in Epithelial and Mesenchymal Composition. *Science* **2013**, *339*, 580−584.
(9) Yu, M.; Stott, S.; Toner, M.; Maheswaran, S.; Haber, D. A. Circulating Tumor Cells: Approaches to Isolation and Characterization. *J. Cell Biol.* **2011**, *192*, 373−382.
(10) Jin, C.; McFaul, S. M.; Duffy, S. P.; Deng, X.; Tavassoli, P.; Black, P. C.; Ma, H. Technologies for Label-Free Separation of Circulating Tumor Cells: From Historical Foundations to Recent Developments. *Lab Chip* **2014**, *14*, 32−44.
(11) Hardingham, J. E.; Kotasek, D.; Farmer, B.; Butler, R. N.; Mi, J.-X.; Sage, R. E.; Dobrovic, A. Immunobead-PCR: A Technique for the Detection of Circulating Tumor Cells Using Immunomagnetic Beads and the Polymerase Chain Reaction. *Cancer Res.* **1993**, *53*, 3455−3458.
(12) Nagrath, S.; Sequist, L. V.; Maheswaran, S.; Bell, D. W.; Irimia, D.; Ulkus, L.; Smith, M. R.; Kwak, E. L.; Digumarthy, S.; Muzikansky, A.; Ryan, P.; Balis, U. J.; Tompkins, R. G.; Haber, D. A.; Toner, M. Isolation of Rare Circulating Tumour Cells in Cancer Patients by Microchip Technology. *Nature* **2007**, *450*, 1235−1239.
(13) Grover, P.; Cummins, A.; Price, T.; Roberts-Thomson, I.; Hardingham, J. Circulating Tumour Cells: The Evolving Concept and the Inadequacy of Their Enrichment by EpCAM-based Methodology for Basic and Clinical Cancer Research. *Ann. Oncol.* **2014**, *25*, 1506−1516.
(14) Joosse, S. A.; Hannemann, J.; Spotter, J.; Bauche, A.; Andreas, A.; Muller, V.; Pantel, K. Changes in Keratin Expression During Metastatic Progression of Breast Cancer: Impact on the Detection of Circulating Tumor Cells. *Clin. Cancer Res.* **2012**, *18*, 993−1003.
(15) Mikolajczyk, S. D.; Millar, L. S.; Tsinberg, P.; Coutts, S. M.; Zomorrodi, M.; Pham, T.; Bischoff, F. Z.; Pircher, T. J. Detection of EpCAM-Negative and Cytokeratin-Negative Circulating Tumor Cells in Peripheral Blood. *J. Oncol.* **2011**, *2011*, 252361.
(16) Zheng, Q.; Iqbal, S. M.; Wan, Y. Cell Detachment: Post-Isolation Challenges. *Biotechnol. Adv.* **2013**, *31*, 1664−1675.
(17) Harouaka, R. A.; Nisic, M.; Zheng, S. Y. Circulating Tumor Cell Enrichment Based on Physical Properties. *J. Lab. Autom.* **2013**, *18*, 455−468.
(18) Guo, Q.; Park, S.; Ma, H. Microfluidic Micropipette Aspiration for Measuring the Deformability of Single Cells. *Lab Chip* **2012**, *12*, 2687−2695.
(19) Zhang, W.; Kai, K.; Choi, D. S.; Iwamoto, T.; Nguyen, Y. H.; Wong, H.; Landis, M. D.; Ueno, N. T.; Chang, J.; Qin, L. Microfluidics Separation Reveals the Stem-Cell-Like Deformability of Tumor-Initiating Cells. *Proc. Natl. Acad. Sci. U.S.A.* **2012**, *109*, 18707−18712.
(20) Hofman, V. J.; Ilie, M. I.; Bonnetaud, C.; Selva, E.; Long, E.; Molina, T.; Vignaud, J. M.; Flejou, J. F.; Lantuejoul, S.; Piaton, E.; Butori, C.; Mourad, N.; Poudenx, M.; Bahadoran, P.; Sibon, S.; Guevara, N.; Santini, J.; Venissac, N.; Mouroux, J.; Vielh, P.; Hofman, P. M. Cytopathologic Detection of Circulating Tumor Cells Using the Isolation by Size of Epithelial Tumor Cell Method Promises and Pitfalls. *Am. J. Clin. Pathol.* **2011**, *135*, 146−156.
(21) Asghar, W.; Wan, Y.; Ilyas, A.; Bachoo, R.; Kim, Y. T.; Iqbal, S. M. Electrical Fingerprinting, 3D Profiling, and Detection of Tumor Cells with Solid-State Micropores. *Lab Chip* **2012**, *12*, 2345−2352.
(22) Lim, L. S.; Hu, M.; Huang, M. C.; Cheong, W. C.; Gan, A. T.; Looi, X. L.; Leong, S. M.; Koay, E. S.; Li, M. H. Microsieve Lab-Chip Device for Rapid Enumeration and Fluorescence in Situ Hybridization of Circulating Tumor Cells. *Lab Chip* **2012**, *12*, 4388−4396.
(23) Marrinucci, D.; Bethel, K.; Kolatkar, A.; Luttgen, M. S.; Malchiodi, M.; Baehring, F.; Voigt, K.; Lazar, D.; Nieva, J.; Bazhenova, L.; Ko, A. H.; Korn, W. M.; Schram, E.; Coward, M.; Yang, X.; Metzner, T.; Lamy, R.; Honnatti, M.; Yoshioka, C.; Kunken, J.; Petrova, Y.; Sok, D.; Nelson, D.; Kuhn, P. Fluid Biopsy in Patients with Metastatic Prostate, Pancreatic, and Breast Cancers. *Phys. Biol.* **2012**, *9*, 016003.
(24) Wang, L. X.; Asghar, W.; Demirci, U.; Wan, Y. Nanostructured Substrates for Isolation of Circulating Tumor Cells. *Nano Today* **2013**, *8*, 374−387.
(25) Chen, W. Q.; Weng, S. N.; Zhang, F.; Allen, S.; Li, X.; Bao, L. W.; Lam, R. H. W.; Macoska, J. A.; Merajver, S. D.; Fu, J. P. Nanoroughened Surfaces for Efficient Capture of Circulating Tumor Cells without Using Capture Antibodies. *ACS Nano* **2013**, *7*, 566−575.
(26) Fischer, J. C.; Niederacher, D.; Topp, S. A.; Honisch, E.; Schumacher, S.; Schmitz, N.; Zacarias Fohrding, L.; Vay, C.; Hoffmann, I.; Kasprowicz, N. S.; Hepp, P. G.; Mohrmann, S.; Nitz, U.; Stresemann, A.; Krahn, T.; Henze, T.; Griebsch, E.; Raba, K.; Rox, J. M.; Wenzel, F.; Sproll, C.; Janni, W.; Fehm, T.; Klein, C. A.; Knoefel, W. T.; Stoecklein, N. H. Diagnostic Leukapheresis Enables Reliable Detection of Circulating Tumor Cells of Nonmetastatic Cancer Patients. *Proc. Natl. Acad. Sci. U.S.A.* **2013**, *110*, 16580−16585.
(27) Zeiger, A. S.; Hinton, B.; Van Vliet, K. J. Why the Dish Makes A Difference: Quantitative Comparison of Polystyrene Culture Surfaces. *Acta Biomater* **2013**, *9*, 7354−7361.
(28) Ishizaki, T.; Saito, N.; Takai, O. Correlation of Cell Adhesive Behaviors on Superhydrophobic, Superhydrophilic, and Micropatterned Superhydrophobic/Superhydrophilic Surfaces to Their Surface Chemistry. *Langmuir* **2010**, *26*, 8147−8154.
(29) Wan, Y.; Kim, Y. T.; Li, N.; Cho, S. K.; Bachoo, R.; Ellington, A. D.; Iqbal, S. M. Surface-Immobilized Aptamers for Cancer Cell Isolation and Microscopic Cytology. *Cancer Res.* **2010**, *70*, 9371−9380.
(30) Wan, Y.; Mahmood, M. A.; Li, N.; Allen, P. B.; Kim, Y. T.; Bachoo, R.; Ellington, A. D.; Iqbal, S. M. Nanotextured Substrates with Immobilized Aptamers for Cancer Cell Isolation and Cytology. *Cancer* **2012**, *118*, 1145−1154.
(31) Keddie, J. L.; Jones, R. A. L.; Cory, R. A. Size-Dependent Depression of the Glass-Transition Temperature in Polymer-Films. *Europhys. Lett.* **1994**, *27*, 59−64.
(32) Wong, C. W.; Lee, A.; Shientag, L.; Yu, J.; Dong, Y.; Kao, G.; Al-Mehdi, A. B.; Bernhard, E. J.; Muschel, R. J. Apoptosis: An Early Event in Metastatic Inefficiency. *Cancer Res.* **2001**, *61*, 333−338.
(33) Ko, T. J.; Kim, E.; Nagashima, S.; Oh, K. H.; Lee, K. R.; Kim, S.; Moon, M. W. Adhesion Behavior of Mouse Liver Cancer Cells on Nanostructured Superhydrophobic and Superhydrophilic Surfaces. *Soft Matter* **2013**, *9*, 8705−8711.
(34) Liu, X.; Chen, L.; Liu, H.; Yang, G.; Zhang, P.; Han, D.; Wang, S.; Jiang, L. Bio-Inspired Soft Polystyrene Nanotube Substrate for Rapid and Highly Efficient Breast Cancer-cell Sapture. *NPG Asia Mater.* **2013**, *5*, e63.
(35) Hallab, N.; Bundy, K.; O'connor, K.; Clark, R.; Moses, R. Cell Adhesion to Biomaterials: Correlations Between Surface Charge, Surface Roughness, Adsorbed Protein, and Cell Morphology. *J. Long-Term Eff. Med. Implants* **1994**, *5*, 209−231.
(36) Chang, X. Z.; Li, D. Q.; Hou, Y. F.; Wu, J.; Lu, J. S.; Di, G. H.; Jin, W.; Ou, Z. L.; Shen, Z. Z.; Shao, Z. M. Identification of the Functional Role of AF1Q in the Progression of Breast Cancer. *Breast Cancer Res. Treat.* **2008**, *111*, 65−78.

(37) Williams, A.; Lin, H.; Datar, R.; Cote, R. J. Reporting the Capture Efficiency of A Filter-Based Microdevice: A CTC Is Not a CTC Unless It Is CD45 Negative. *Clin. Cancer Res.* **2011**, *17*, 3050.